Treatment of the Multimode Jahn−Teller Problem in Small Aromatic Radicals

Maja Gruden-Pavlović,[†] Pablo García-Fernández,[‡] Ljubica Andjelković,[§] Claude Daul,[||] and Matija Zlatar*,[§]

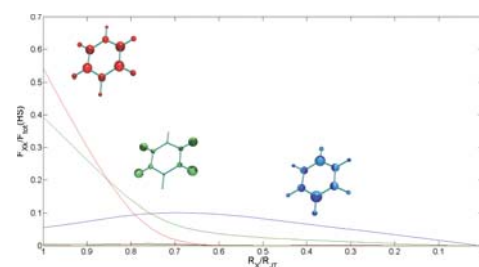[†]Faculty of Chemistry, University of Belgrade, Belgrade, Serbia

[‡]Ciencias de la Tierra y Física de la Materia Condensada, Universidad de Cantabria, Santander, Spain

[§]Center for Chemistry, IHTM, University of Belgrade, Belgrade, Serbia

[||]Department of Chemistry, University of Fribourg, Fribourg, Switzerland

Ⓢ *Supporting Information*

ABSTRACT: The family of the Jahn−Teller (JT) active hydrocarbon rings, C_nH_n ($n = 5-7$), was analyzed by the means of multideterminantal density functional theory (DFT) approach. The multimode problem was addressed using the intrinsic distortion path (IDP) method, in which the JT distortion is expressed as a linear combination of all totally symmetric normal modes in the low symmetry minimum energy conformation. Partitioning of the stabilization energy into the various physically meaningful terms arising from Kohn−Sham DFT has been performed to get further chemical insight into the coupling of the nuclear movements and the electron distribution.

◼ INTRODUCTION

Jahn−Teller (JT) type distortions include proper JT distortions of molecules in a degenerate electronic state,[1] pseudo JT (PJT) distortions in a nondegenerate electronic states,[2] and Renner−Teller (RT) distortions in a linear systems.[3] Any structural distortion of a polyatomic system is, as a consequence, of the JT, PJT, or RT origin.[2] The distortion influences various molecular properties and plays an essential role in molecular stereochemistry, chemical activation, reactivity, and mechanisms of chemical reactions, electron-conformational effects in biological systems, phase transitions in condensed matter, and so forth. Literature is abundant with details about the theory and various problems in modern chemistry and solid-state physics, that have been successfully explained within the framework of the JT effect.[2,4] The JT effect is crucial in the explanation of different phenomena, for example, the high-T_C superconductivity[5] or the colossal magnetoresistance in manganites.[6] Accordingly, these are the reasons why, even though it passed over 70 years from the publication of the seminal paper of Jahn and Teller,[1] this effect continues to be a subject of interest in various fields of chemistry and physics.

The Jahn−Teller (JT) theorem states that a molecule with a degenerate electronic state distorts along nontotally symmetric vibrational coordinates. This removes the degeneracy and lowers the energy. Near the point of electronic degeneracy the Born−Oppenheimer (BO), or adiabatic, approximation breaks down, and there is a coupling between electronic states and nuclear motion. Although, the concept of the potential energy surface, strictly speaking, loses its physical meaning of the potential energy of the nuclei, traditional computational methods, can still be used, if a perturbation approach is introduced to the BO
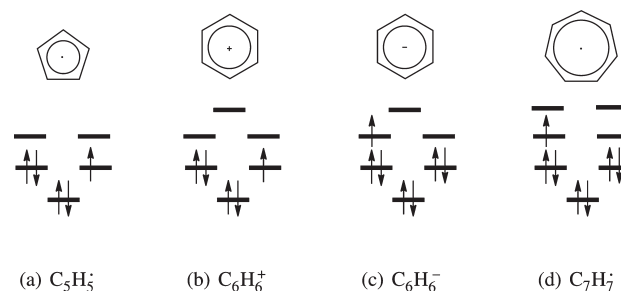

(a) $C_5H_5^{\cdot}$ (b) $C_6H_6^{+}$ (c) $C_6H_6^{-}$ (d) $C_7H_7^{\cdot}$

Figure 1. Molecules studied in this work; a simple molecular orbital scheme is outlined.

approximation. In this way all of the standard concepts in theoretical chemistry are still useful for the elucidation and prediction of the properties of the JT active molecules, and many manifestations of the JT effect can be understood within the BO approximation.

The cyclopentadienyl radical ($C_5H_5^{\cdot}$), benzene cation ($C_6H_6^{+}$), benzene anion ($C_6H_6^{-}$), and tropyl radical ($C_7H_7^{\cdot}$) are important species in organic chemistry but also are very interesting for spectroscopic and quantum chemistry studies. All of them have a single electron or a hole in a doubly degenerate highest occupied molecular orbital, leading to a degenerate state arising as a consequence of an addition or removal of an electron in the parent aromatic molecule, as in Figure 1. Hence, these molecules are JT unstable and distort to conformations of lower

symmetry. Moreover, $C_5H_5^{\bullet}$ and $C_6H_6^{+}$ are paradigmatic examples of the dynamic JT effect. These two molecules are certainly most studied in the C_nH_n family, both experimentally and theoretically.[7−17] Comparing to $C_5H_5^{\bullet}$ and $C_6H_6^{+}$, information on the properties of $C_6H_6^{-}$ and $C_7H_7^{\bullet}$ is relatively sparse.[14,15,18−21]

In this paper, results obtained by multideterminantal density functional theory (DFT) procedure[22] for a detailed interpretation of JT type distortions in this family of organic radicals are presented. The analysis of the structural distortion from the high symmetry (HS) nuclear arrangements of these molecules presents a challenge because of the superposition of the effects produced by many different normal modes. To tackle this problem, we have recently proposed to express the JT distortion as a linear combination of all totally symmetric normal modes in the low symmetry (LS) minimum energy conformation.[11] The basis of the method is to represent the distortion along the steepest descent path from the HS point to the LS minimum projecting the geometry of the system on the normal modes of the LS configuration. This allows quantification of the importance of all of the involved normal modes along a relevant particular path of distortion.

The aim of the present work was to calculate reliable values of the JT parameters in this family of molecules, trying to clarify, at the same time, the role played by the different symmetry-breaking and totally symmetric normal modes in the global distortion. To expand on our previous works[11,23] the structural analysis is complemented by analyzing the role played by the different electronic interactions (electron−nuclei, electron−electron, etc.) present in the Hamiltonian leading to a more complete and balanced view of the changes undergone by the system along the JT distortion. As shown in the Results and Discussion section, we have found that the JT relaxation in multimode problems occurs in two well-differentiated phases. The first phase is governed by the electron−nuclear interactions, as it is typical for the JT problems. In a second phase changes in the electron density, driven by the PJT effect, significantly modify the kinetic and electron−electron contributions to the total energy.

■ THEORETICAL METHODS

Consider a nonlinear N-atomic molecule in the HS nuclear configuration, $\vec{R}_{HS}$, with a degenerate electronic state, which spans the irreducible representation Γ_{el} of a HS point group. $\mathscr{H}_{HS}$ is the electronic Hamiltonian, which defines the electronic structure at $\vec{R}_{HS}$. The molecule has $3N − 6$ normal coordinates $\vec{Q}_k$, where $k = 1, ..., 3N − 6$ ($3N − 5$ for the of linear molecules) which can be classified according to the corresponding irreducible representations of the HS point group. To discuss the shape of the adiabatic potential energy surface, the electronic Hamiltonian, $\mathscr{H}$, is expanded as a Taylor series around $\vec{R}_{HS}$, along the $\vec{Q}_k$:
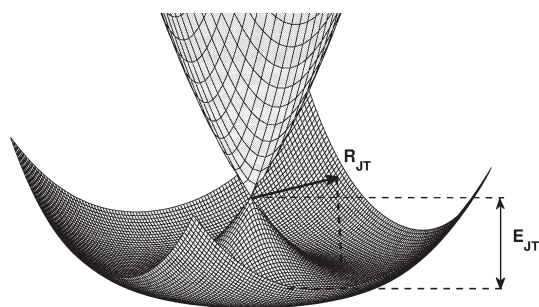
$$\mathscr{H} = \mathscr{H}_{HS} + \sum_{k=1}^{3N-6} \left(\frac{\partial \mathscr{V}}{\partial \vec{Q}_k} \right)_{HS} \vec{Q}_k$$

$$+ \frac{1}{2} \sum_{k,l=1}^{3N-6} \left(\frac{\partial^2 \mathscr{V}}{\partial \vec{Q}_k \partial \vec{Q}_l} \right)_{HS} \vec{Q}_k \vec{Q}_l + \cdots \quad (1)$$

The coefficients in the perturbational expression of the potential energy, within the basis of degenerate electronic state, are vibronic coupling coefficients. These matrix elements measure the coupling between the electronic states through the nuclear motions. The irreducible representations of the nontotally symmetric, JT active modes, must belong to the same
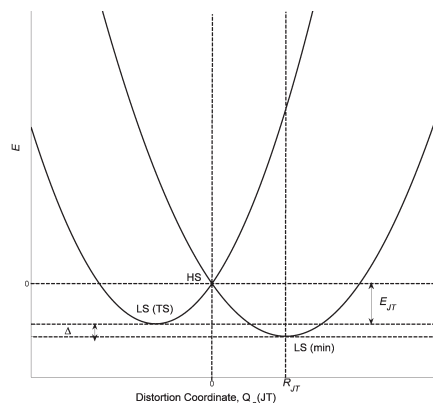
representation as the symmetric direct product of the components of the degenerate electronic state, $\Gamma_{JT} = [\Gamma_{el} \times \Gamma_{el}] − A_1$. The JT problems are classified according to the symmetry types of the electronic states and the vibrations that are coupled. The molecules considered in this work, in the HS nuclear configuration, have a doubly degenerate electronic ground state which is coupled with a doubly degenerate vibrations; that is, they belong to the $E \otimes e$ problem. The point group of the LS minimum energy conformation is defined by the requirement that the irreducible representations (irreps) of the active modes become totally symmetric upon descent in symmetry and the application of the epikernel principle.[2,24] The adiabatic potential energy surface has a Mexican-hat-like shape, depicted for the case of one-mode $E \otimes e$ JT problem in Figure 2a. A qualitative cut through the adiabatic potential energy surface, along the JT active distortion Q_a, is given in Figure 2b. The figure indicates how the parameters E_{JT} (the JT stabilization energy), Δ (the warping barrier), and R_{JT} (the JT radius) define the adiabatic potential energy surface. Warping of the adiabatic potential surface occurs if $\Delta \neq 0$ and is due to the higher order (second order, anharmonicity, etc.) or PJT terms in the perturbational expression, eq 1.[25] To determine this set of parameters, it is necessary to perform either an experiment and fit the results to the proposed model or to carry out a computational study, for example, DFT calculations.

Complications arise when we have more than one vibration responsible for the distortion, a typical scenario when considering polyatomic molecules and almost a certainty when dealing with solid-state problems. As the dimension of the problem becomes much higher, the Mexican-hat representation of the adiabatic potential energy surface is not appropriate anymore for the description of the distortion, and new effects may arise. The appraisal of the influence of different normal modes on the JT effect is referred to as a multimode problem. In previous approaches,[2] the multimode problem was reduced to the so-called interaction mode where the displacement from the HS cusp to the LS minimum is performed along a straight line in a normal-mode space, leading to an energy surface with qualitatively the same shape as the one-mode problem. While this method allows for a qualitative feeling of the nature of the JT effect, it gives very little information on the role played by each of the distortion modes. In particular, while each of the active vibrations is characterized with a set of vibronic coupling constants or, in the other words, with its own Mexican-hat type adiabatic potential energy surface, the final JT effect cannot be understood as a simple superposition of the effects of individual active modes. Alternatively to the method utilizing HS symmetrized coordinates,[2,26] we have recently proposed to analyze the multimode problem by expressing the distortion along the minimal energy path, intrinsic distortion path (IDP), from the HS point to the LS distorted minimum, projecting the geometry of the system on the LS normal modes.[11] The reduction of the multimode problem to either interaction mode or IDP solves the structural part of the problem, that is, static JT effect and analysis of the adiabatic potential energy surfaces, but not the dynamical part, meaning the changes in vibrational frequencies by the multimode distortion and calculation of the vibronic wave functions. A dynamical multimode problem has been described in detail in the literature.[2,16,17]

In the subsequent parts of this section, we will give a concise retrospective of the multideterminantal DFT procedure for the

(a) 3-dimensional representation, $\Delta = 0$

(b) cut through the adiabatic potential energy surface, along the JT active distortion, $\Delta \neq 0$

Figure 2. Indication of the JT parameters: the JT stabilization energy, E_{JT}, the JT radius, R_{JT}, the warping barrier, Δ; 3D representation of the adiabatic potential energy surface for the $E \otimes e$ JT problem, when $\Delta = 0$ (part a).

calculations of the JT parameters,[11,22] followed by the description of the IDP approach[11] to the multimode JT problem, the DFT based energy partitioning scheme[27] employed to analyze the stabilization due to the multimode JT effect, and finally the summary of the Theoretical Methods section within the force approach to the JT effect.[28,29]

Multideterminantal DFT Approach. The method for calculations of the JT parameters, in Figure 2a,b, by means of DFT in a recent past has been successfully applied with a good accuracy for the analysis of the JT active molecules.[11,22,23,30−33] Briefly, it is necessary to know geometries and energies of the HS and LS nuclear configurations. For the LS structure, as the system is in a nondegenerate electronic ground state, this is unambiguous. The electronic structure of the HS point, on the other hand, must be represented with at least two Slater determinants or use some constrained electron configuration method.[32] Consequently, using a single determinant DFT is troublesome.[30,34,35] A method based on the multideterminantal DFT is therefore used here. This procedure consists of the following steps:

(i) Average of configuration (AOC) type calculation in the HS point group. This yields a geometry of the HS species.

(ii) A single-point calculation imposing the high symmetry on the nuclear geometry and the low symmetry on the electron density. This gives the energy of a Slater determinant with an integer electron orbital occupancy.

(iii) A geometry optimization constraining the structure to the LS point group, with the proper occupancy of Kohn−Sham (KS) orbitals. These calculations yield different geometries and energies that correspond to a minimum and a transition state on the adiabatic potential energy surface. The difference in energies between these structures gives the warping barrier, Δ.

(iv) The JT stabilization energy, E_{JT}, is the difference between the energies obtained in the steps ii and iii.

(v) R_{JT} is given by the length of the distortion vector between the HS and the LS minimum energy configurations.

This computational procedure for the particular example of the JT effect in $C_5H_5^{\bullet}$ is summarized in Figure 3.
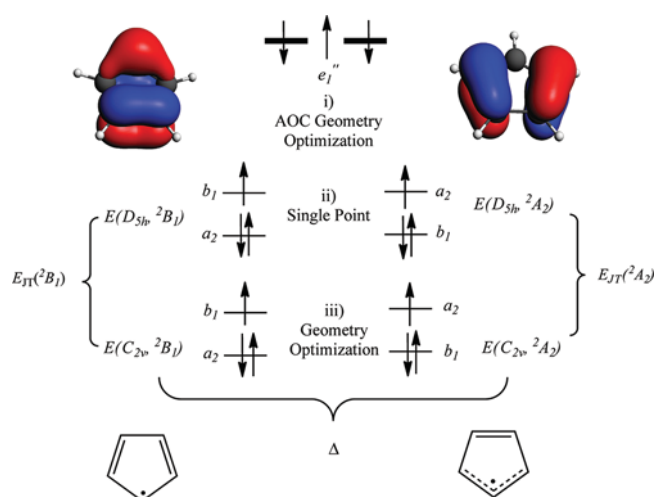

Figure 3. Multideterminantal DFT approach for the calculation of the JT parameters for the $D_{5h} \rightarrow C_{2v}$ distortion of $C_5H_5^{\bullet}$; single occupied molecular orbitals are shown.

The DFT calculations have been carried out using the Amsterdam Density Functional program package, ADF2009.01.[36] The local density approximation (LDA) characterized by the Vosko−Wilk−Nusair (VWN)[37] parametrization have been used for the symmetry constrained geometry optimizations. An all-electron triple-zeta Slater-type orbitals (STO) plus one polarization function (TZP) basis set has been used for all atoms. All calculations were spin-unrestricted. Separation of the orbital and the geometrical symmetry, as used in the calculation of the energies of the HS nuclear configurations, step ii, is done using SYMROT subblock in the QUILD program, version 2009.01,[38] provided in the ADF2009.01 program package. Analytical harmonic frequencies[39] and normal modes at the LS stationary points were calculated.

Intrinsic Distortion Path. In general, the JT distortion is a superposition of many different normal coordinates. In the LS point group JT active modes might mix with a_1 vibrations, which are always present in the direct product and never change upon descent in symmetry. In some situations, other irreps in

3

Table 1. Summary of the Group Theory Considerations for the JT Distortions in $C_5H_5^\bullet$, $C_6H_6^+$ and $C_7H_7^{\bullet}$ [a]

	distortion	Γ_{el}	Γ_{JT}	$3N-6$	N_{a_1}	origin of the LS a_1 vibs[b]
$C_5H_5^\bullet$	$D_{5h} \to C_{2v}$	$E''_1 \to A_2 + B_1$	$E'_2 \to A_1 + B_2$	24	9	$4e'_2, 2a'_1, 3e'_1$
$C_6H_6^+$	$D_{6h} \to D_{2h}$	$E_{1g} \to B_{2g} + B_{3g}$	$E_{2g} \to A_g + B_{1g}$	30	6	$4e_{2g}, 2a_{1g}$
$C_7H_7^\bullet$	$D_{7h} \to C_{2v}$	$E''_2 \to A_2 + B_1$	$E'_3 \to A_1 + B_2$	36	13	$4e'_3, 4e'_2, 3e'_1, 2a'_1$

[a] Γ_{el} is irrep of the electronic state; Γ_{JT} is irrep of the JT active vibrations; N is the number of atoms in a molecule; N_{a1} is the number of totally symmetrical vibrations in the LS point group. [b] One component of the degenerate pairs of vibrations in the HS becomes a_1 in the LS point group.

Table 2. Results of the DFT Calculations Performed To Analyze the JT Effect in $C_6H_6^+$ [a]

occupation	state	geometry	energy
$e_{1g}^{0.75} e_{1g}^{0.75}$	$^2E_{1g}$	D_{6h}	-70.9461
$b_{3g}^2 b_{2g}^1$	$^2B_{2g}$	D_{6h}	-70.9122
$b_{2g}^2 b_{3g}^1$	$^2B_{3g}$	D_{6h}	-70.9141
$b_{3g}^2 b_{2g}^1$	$^2B_{2g}$	D_{2h}	-71.0212
$b_{2g}^2 b_{3g}^1$	$^2B_{3g}$	D_{2h}	-71.0172
E_{JT}	$^2B_{2g}$		879.2
E_{JT}	$^2B_{3g}$		831.6
Δ			32.2
R_{JT}	$^2B_{2g}$		0.27
R_{JT}	$^2B_{3g}$		0.27
$E_{JT}(IDP)$	$^2B_{2g}$		839.1
$E_{JT}(IDP)$	$^2B_{3g}$		791.1

[a] Energies (LDA) are given in eV; the JT parameters E_{JT} and Δ are given in cm^{-1} and R_{JT} in $(amu)^{1/2}$ Å.

Table 3. Results of the DFT Calculations Performed To Analyze the JT Effect in $C_7H_7^\bullet$ [a]

occupation	state	geometry	energy
$e''_2{}^{0.5} e''_2{}^{0.5}$	$^2E''_2$	D_{7h}	-91.8973
$a_2^1 b_1^0$	$^2A_2$	D_{7h}	-91.8968
$a_2^0 1b_1^1$	$^2B_1$	D_{7h}	-91.8968
$a_2^1 b_1^0$	$^2A_2$	C_{2v}	-92.0026
$a_2^0 1b_1^1$	$^2B_1$	C_{2v}	-92.0026
E_{JT}	$^2A_2$		853.3
E_{JT}	$^2B_1$		853.3
Δ			0.0
R_{JT}	$^2A_2$		0.16
R_{JT}	$^2B_1$		0.16
$E_{JT}(IDP)$	$^2A_2$		861.2
$E_{JT}(IDP)$	$^2B_1$		862.2

[a] Energies (LDA) are given in eV; the JT parameters E_{JT} and Δ are given in cm^{-1} and R_{JT} in $(amu)^{1/2}$ Å.

the HS point group, which are not contained in the direct product, may become totally symmetric upon descent in symmetry and therefore contribute to the JT distortion also. This is found in the case of the JT $D_{5h} \to C_{2v}$ distortion for $C_5H_5^\bullet$ and $D_{7h} \to C_{2v}$ distortion for $C_7H_7^\bullet$. The normal coordinates that are basis of the e'_2, e'_1, and a'_1 irreducible representations in D_{5h} and e'_3, e'_2, e'_1, and a'_1 in D_{7h} become totally symmetric in C_{2v}.

In the IDP model,[11] the geometry of the LS energy minimum is chosen to be the origin of the configuration space, $\vec{R}_{LS} = \vec{0}$. This conformation is a true minimum on the adiabatic potential energy surface and has the property that the Hessian of the energy is positive semidefinite; thus it can be used to obtain the harmonic vibrational modes without any complications.

Every point on the potential energy surface can be represented by a $3N$ dimensional vector $\vec{R}_X$ using mass-weighted generalized coordinates relative to the origin. In the harmonic approximation, it is possible to express R_X as a linear combination of all totally symmetric normal coordinates (N_{a1}) from the LS energy minimum conformation:

$$\vec{R}_X = \mathbf{Q} \, \vec{w}_X \tag{2}$$

where $\mathbf{Q}$ is the $3N \times N_{a1}$ matrix with a columns being mass-weighted totally symmetric normal coordinates, obtained by the DFT calculations in the LS minimum energy conformation. $\vec{w}_X$ is the N_{a1} dimensional vector containing the weighting factors, w_{Xk}, which can be easily obtained solving the linear problem, eq 2. w_{Xk} represent the contribution of the displacements along the totally symmetric normal coordinate Q_k, to the $\vec{R}_X$. The energy of the nuclear configuration R_X, E_X, relative to the energy of the origin,

in harmonic approximation, is expressed as the sum of the energy contributions of all N_{a1} LS totally symmetric normal coordinates:
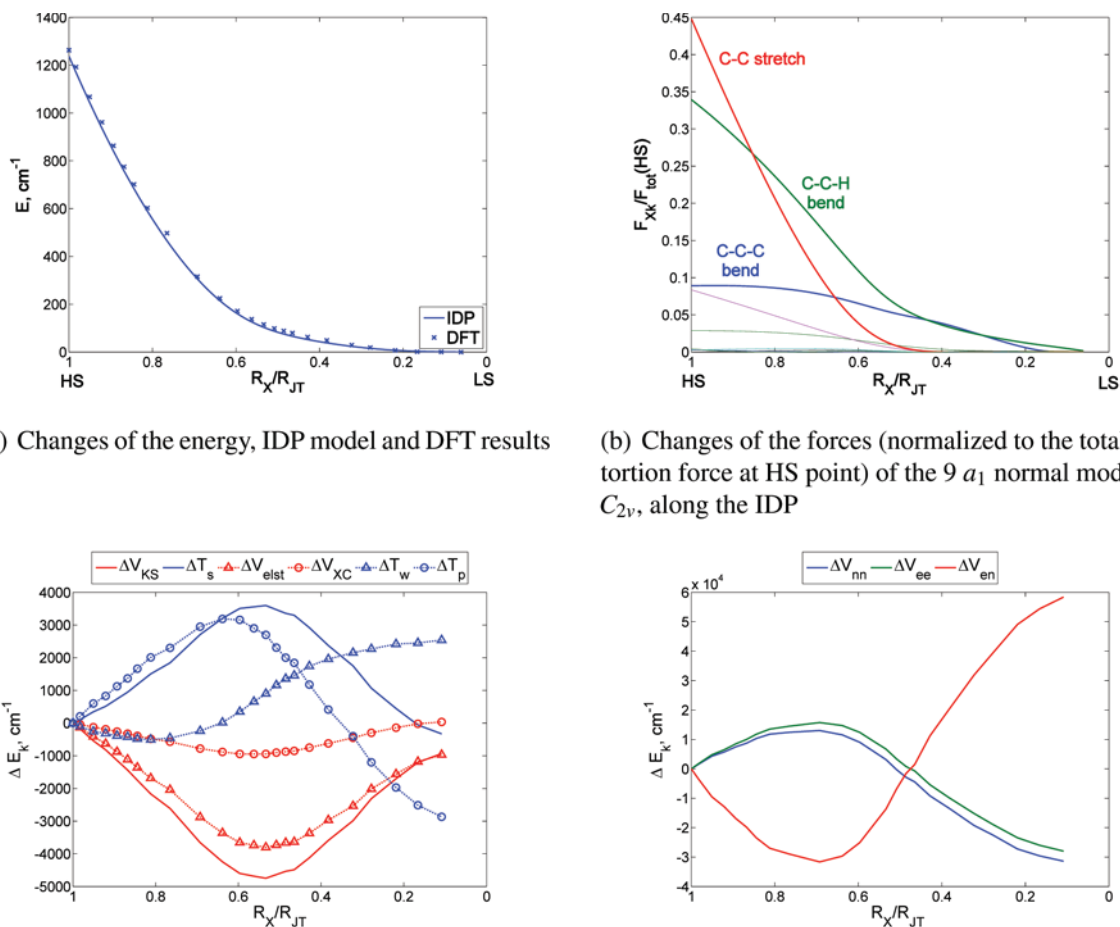
$$E_X = \sum_{k=1}^{N_{a1}} E_{kX} = \frac{1}{2} \sum_{k=1}^{N_{a1}} w_{Xk}^2 \, \vec{Q}_k{}^2 \lambda_k \tag{3}$$

where λ_k are the eigenvalues of the Hessian from the DFT calculations in the LS minimum energy conformation. Using these considerations, eqs 2 and 3, we can analyze the multimode JT problem by expressing the $\vec{R}_{JT}$ as a superposition of all of the LS totally symmetric normal coordinates and directly obtaining the energy contributions of all of the normal modes to the total stabilization energy:

$$\vec{R}_{JT} = \mathbf{Q} \, \vec{w}_{kJT} \tag{4}$$

$$E_{JT} = \sum_{k=1}^{N_{a1}} E_{kJT} = \frac{1}{2} \sum_{k=1}^{N_{a1}} w_{kJT}^2 \, \vec{Q}_k{}^2 \lambda_k \tag{5}$$

The vector $\vec{R}_{JT} = \vec{R}_{HS}$ defines the straight path from the HS point to the LS minimum. The direct path contains essential information on the vibronic coupling at the HS point and is equivalent to the interaction mode of Bersuker et al.[2,26] This direct path is in general different from the minimal energy path from the HS point on the potential energy surface to the LS global minimum. The force along the normal mode Q_k, F_{Xk}, which drives the nuclei along that coordinate to the minimum, at any point $\vec{R}_X$ is defined as a derivative of the energy over the Cartesian coordinates. In the HS point this will lead information about the main driving force for the JT distortion from the HS to

(a) Changes of the energy, IDP model and DFT results

(b) Changes of the forces (normalized to the total distortion force at HS point) of the 9 a_1 normal modes in C_{2v}, along the IDP

(c) Changes of the potential, kinetic energies, and their components along the IDP

(d) Changes of the different electrostatic energy terms along the IDP

Figure 4. Intrinsic distortion path and energy component analysis of the JT $D_{5h} \rightarrow C_{2v}$ distortion in $C_5H_5^{\bullet}$.

the LS. The total distortion force, $\vec{F}_{\mathrm{Xtot}}$, is given as a vector sum of the individual forces. $\vec{F}_{\mathrm{Xtot}}$ gives the direction from one to the another point on the adiabatic potential energy surface in a steepest descent way:

$$\vec{F}_{\mathrm{Xtot}} = \sum_{k=1}^{N_{a_1}} \vec{F}_{\mathrm{X}k} = \sum_{k=1}^{N_{a_1}} w_{\mathrm{X}k} \lambda_k \mathbf{M}^{1/2} \vec{Q}_k \quad (6)$$

where $\mathbf{M}$ is a diagonal $3N \times 3N$ matrix with atomic masses in triplicates as elements ($m_1, m_1, m_1, m_2, ..., m_N$).

Matlab scripts for the IDP analysis and for the extraction of necessary data from the ADF frequency calculations can be obtained from authors upon request. To correlate the vibrations in the LS structure with vibrations in the HS, a model developed by Hug and Fedorovsky was used.[40]

Energy Component Analysis. In the time-independent, nonrelativistic, BO approximation, the molecular Hamiltonian operator, $\mathcal{H}$, consists of a sum of the electron kinetic energy ($\mathcal{T}$), the nuclear−nuclear Coulomb repulsion ($\mathcal{V}_{\mathrm{nn}}$), the electron−nuclear interaction ($\mathcal{V}_{\mathrm{en}}$), and the electron−electron repulsion ($\mathcal{V}_{\mathrm{ee}}$) operators. Thus, the energy of a system, which is the expectation value of the Hamiltonian operator, can be expressed as a sum of the expectation values of the corresponding operators:

$$E = T + V_{\mathrm{en}} + V_{\mathrm{ee}} + V_{\mathrm{nn}} \quad (7)$$
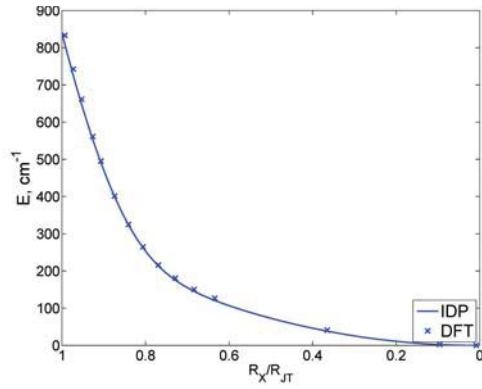
All of the quantities can be calculated with the Hartree−Fock, post Hartree−Fock, or DFT approaches. An analysis of the changes of these energy components during a chemical transformation helps to understand the nature of chemical bonding in a molecule. The studies along this line were performed for the analysis of the formation of covalent bonds,[41] to explain the Hund's rule,[42] aromaticity,[43] different spin states of iron complexes,[44] PJT distortions,[45,46] DFT-based quantification of the steric and quantum effects,[27,47] and so forth. Nevertheless, energy component analysis was seldom used for the analysis of the JT effect.[48]

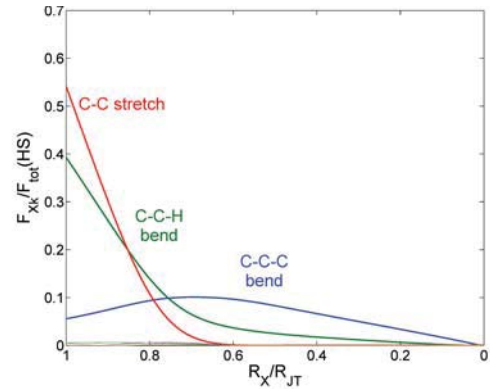Within the KS-DFT formalism,[49,50] changes of the individual energy terms can be formulated as:

$$\begin{aligned} \Delta E &= \Delta T_{\mathrm{s}} + \Delta V_{\mathrm{KS}} \\ &= (\Delta T_{\mathrm{w}} + \Delta T_{\mathrm{p}}) + (\Delta V_{\mathrm{elst}} + \Delta V_{\mathrm{XC}}) \end{aligned} \quad (8)$$

$$\Delta V_{\mathrm{elst}} = \Delta V_{\mathrm{en}} + \Delta J + \Delta V_{\mathrm{nn}} \quad (9)$$
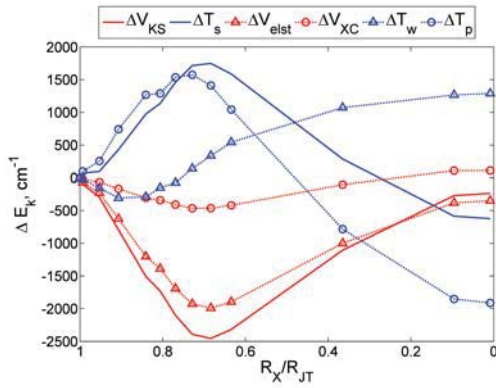
where ΔT_{s} is change of the kinetic energy of a fictitious system of noninteracting electrons and ΔV_{KS} is a change of the KS potential
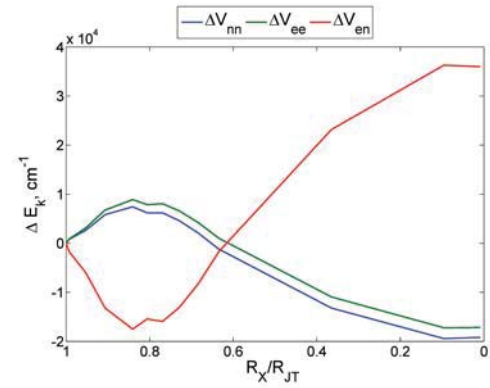
5

(a) Changes of the energy, IDP model and DFT results

(b) Changes of the forces (normalized to the total distortion force at HS point) of the 6 a_g normal modes in D_{2h}, along the IDP

(c) Changes of the potential, kinetic energies, and their components along the IDP

(d) Changes of the different electrostatic energy terms along the IDP

Figure 5. Intrinsic distortion path and energy component analysis of the JT $D_{6h} \rightarrow D_{2h}$ distortion in $C_6H_6^+$.

energy that consists of the changes of the electron—nuclear potential energy (ΔV_{en}), changes of the classical Coulomb electron—electron repulsion (ΔJ), and changes of the exchange-correlation potential energy (ΔV_{XC}). ΔV_{en}, ΔJ, and ΔV_{nn} are conveniently grouped together into the classical electrostatic term, ΔV_{elst}. V_{XC} consists of the residual part of the true kinetic energy, sometimes referred to as the correlation kinetic energy,[50,51] and the nonclassical electrostatic interactions. ΔT_s is partitioned into the changes of the Weizsäcker kinetic energy ΔT_w ($T_w = (1/8) \int (|\nabla \rho(\vec{r})|^2)/(\rho(\vec{r})) d\vec{r}$)[52] and the Pauli kinetic energy ΔT_p.[27,53,54] Liu defined T_w as a steric energy from KS-DFT.[27] T_p, itself simply defined as $T_p = T_s - T_w$, is regarded as an extra kinetic energy required of the fermions by the Pauli exclusion principle.[27] T_w is consistent with Weisskopf's kinetic energy pressure;[55] it is related to Bader's atoms in molecule approach[56] and Fisher information theory.[57] T_p appears in a definition of electron localization function.[58] The fermionic quantum energy contribution can be defined as a $T_p + V_{XC}$.[27] DFT based quantification of the steric, electrostatic, and fermionic quantum energy contributions was applied in the analysis of various chemical problems.[27,47]
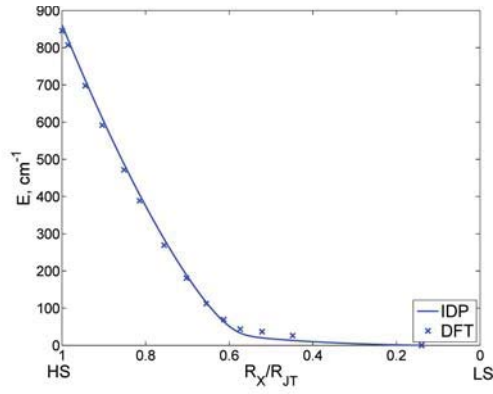
Values of the individual energy components were obtained from single-point LDA calculations, with 6-31G* basis set for all of the atoms, on the geometries obtained from the IDP analysis, using a NWChem program package, version 6.0.[59]

Changes of the Energy Components and the Force Approach to the JT Effect. The origin of the JT effect is a non-null symmetry-breaking force appearing in every nonlinear system in a degenerate electronic state. In general, the force along a general direction $\vec{Q}$ can be written as
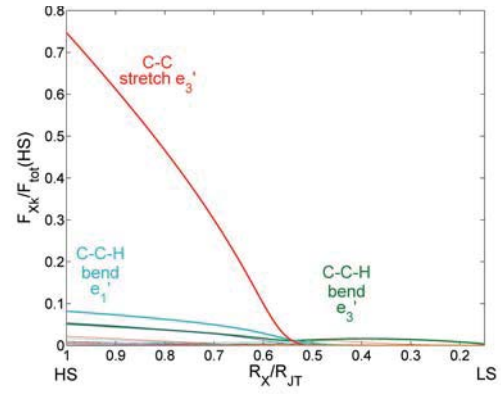
$$\vec{F} = -\frac{\partial E}{\partial \vec{Q}} = -\left(\frac{\partial T}{\partial \vec{Q}} + \frac{\partial V_{en}}{\partial \vec{Q}} + \frac{\partial V_{ee}}{\partial \vec{Q}} + \frac{\partial V_{nn}}{\partial \vec{Q}} \right) \tag{10}$$

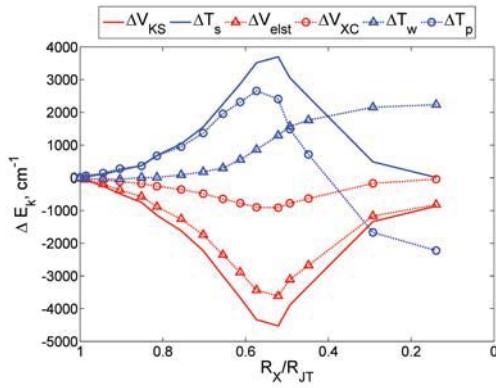but this expression can be simplified using the Hellmann—Feynman or electrostatic theorem[60]

$$\vec{F} = -\frac{\partial E}{\partial \vec{Q}} = -\langle \Psi | \frac{\partial \mathcal{V}}{\partial \vec{Q}} | \Psi \rangle$$

$$= -\left(\langle \Psi | \frac{\partial \mathcal{V}_{en}}{\partial \vec{Q}} | \Psi \rangle + \frac{\partial \mathcal{V}_{nn}}{\partial \vec{Q}} \right)$$

$$= -\left(\int \rho(\vec{r}) \frac{\partial \mathcal{V}_{en}(\vec{r}, \vec{Q})}{\partial \vec{Q}} d\vec{r} + \frac{\partial \mathcal{V}_{nn}}{\partial \vec{Q}} \right) \tag{11}$$
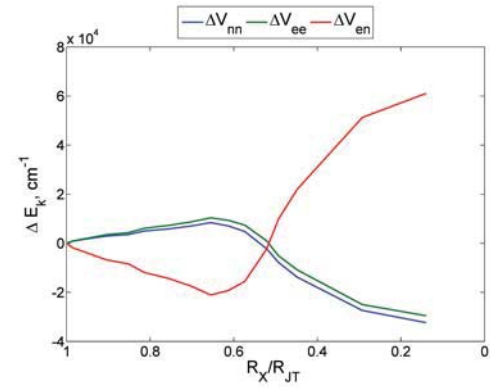
6

(a) Changes of the energy, IDP model and DFT results

(b) Changes of the forces (normalized to the total distortion force at HS point) of the 13 a_1 normal modes in C_{2v}, along the IDP

(c) Changes of the potential, kinetic energies, and their components along the IDP

(d) Changes of the different electrostatic energy terms along the IDP

Figure 6. Intrinsic distortion path and energy component analysis of the JT $D_{7h} \rightarrow C_{2v}$ distortion in $C_7H_7^{\bullet}$.

For the high-symmetry configuration in a JT problem, the first term in eq 11 is called the vibronic coupling constant, while the second is null due to the symmetry considerations. This is the reason why the JT effect is usually considered to have a purely electrostatic origin. However, it must be taken into account that the expected values of all operators included in eq 10 change during a geometry change:

$$\frac{\partial V_{ee}}{\partial \vec{Q}} = \langle \frac{\partial \Psi}{\partial \vec{Q}} | \mathscr{V}_{ee} | \Psi \rangle + \langle \Psi | \mathscr{V}_{ee} | \frac{\partial \Psi}{\partial \vec{Q}} \rangle \qquad (12)$$

$$\frac{\partial T}{\partial \vec{Q}} = \langle \frac{\partial \Psi}{\partial \vec{Q}} | \mathscr{T} | \Psi \rangle + \langle \Psi | \mathscr{T} | \frac{\partial \Psi}{\partial \vec{Q}} \rangle \qquad (13)$$

and the Hellman−Feymann theorem only shows that the force for a particular geometry exclusively depends on the electron−nuclei interaction and electron density for that point, eq 11. After an infinitesimal distortion has taken place in the system due to this force, the electron density is also changed (as expressed, for example through the PJT effect[2]), and all terms in eq 10 start contributing to the changes in energy, as seen trivially, for example when writing the energy functional in DFT. Thus, and as stressed previously in the literature,[61] when discussing the

Table 4. Analysis of the Multimode JT Problem in $C_5H_5^{\bullet}$, $C_6H_6^{+}$, and $C_7H_7^{\bullet}$ by the LS Totally Symmetric Normal Modes in Harmonic Approximation[a]

assignment	molecule	HS-irrep	$\tilde{\nu}_k$ in LS	c_k	E_k
C−C−C bend	$C_5H_5^{\bullet}$	e'_2	831	24.19	19.99
	$C_6H_6^{+}$	e_{1g}	591	51.99	34.33
	$C_7H_7^{\bullet}$	e'_3	894	5.31	1.87
C−C−H bend	$C_5H_5^{\bullet}$	e'_2	1040	52.18	20.02
	$C_6H_6^{+}$	e_{1g}	1166	34.63	16.99
	$C_7H_7^{\bullet}$	e'_3	1234	30.53	3.92
C−C stretch	$C_5H_5^{\bullet}$	e'_2	1482	13.93	53.74
	$C_6H_6^{+}$	e_{1g}	1556	12.40	46.99
	$C_7H_7^{\bullet}$	e'_3	1234	44.07	87.55

[a] Frequencies of selected normal modes are in cm^{-1} as obtained from DFT calculations; contribution of the normal mode $\vec{Q}_k$ to the $\vec{R}_{JT}$ is given by c_k in %; E_k energy contribution of $\vec{Q}_k$ to the E_{JT} in %.

variations of geometry of a particular system one should not consider that the forces are merely electrostatic. As we will see in the Discussion section, in the multimode JT problem different distortion modes play different roles with respect to the terms in

eq 10. In particular, we will find that some modes stabilize the molecule very strongly through the electron−nuclear interactions, while others play more subtle roles allowing the relaxation of electron−electron and kinetic energy terms through changes in the electron density. In rigor, these later terms must be described using the PJT effect,[2] which is not explicitly considered in this work.

■ RESULTS AND DISCUSSION

The ground electronic state of C_5H_5, $C_6H_6^+$, and $C_7H_7^{\bullet}$ in a HS point group belongs to a double degenerate irrep that we will denote Γ_{el}, which splits into two nondegenerate electronic states in for LS point group. This yields two different LS geometries, usually referred as dienyl ($^2B_1$ $C_5H_5^{\bullet}$) and en-alyl ($^2A_2$ $C_5H_5^{\bullet}$) or elongated ($^2B_{2g}$ $C_6H_6^+$, $^2B_1$ $C_7H_7^{\bullet}$) and compressed ($^2B_{3g}$ $C_6H_6^+$, $^2A_2$ $C_7H_7^{\bullet}$) structures. The JT active distortion is the totally symmetric reaction coordinate in the LS point group. The other component of the double degenerate JT active distortion allows mixing of the two electronic states emerging from the degenerate ground state. This is summarized in Table 1.

Multideterminantal DFT calculations of the JT distortion in $C_5H_5^{\bullet}$ revealed a E_{JT} of 1253 cm^{-1}.[11] This value is in an excellent agreement with the experimentally estimated one of 1237 cm^{-1}, in ref 7b. The difference in the energies of the different electronic states in C_{2v} is only 1.6 cm^{-1} which is in the range of precision of the calculations[11] and clearly indicates the existence of a dynamical JT effect. The IDP method gives an E_{JT} of 1238 cm^{-1}.[11]

According to the DFT calculations for $C_6H_6^+$, as seen in Table 2, the $^2B_{2g}$ state is the global minimum on the potential energy surface, more stable than the $^2B_{3g}$ one for $\Delta = 32$ cm^{-1}, and $E_{JT} = 880$ cm^{-1}. A small energy difference between the $^2B_{2g}$ and $^2B_{3g}$ states suggests that the second-order JT effects and anharmonicity are small and that the JT effect in $C_6H_6^+$ is dynamic. These results are in agreement with previous studies, which report the value of E_{JT} between 700 and 1000 cm^{-1}.[13−15] Δ is experimentally estimated to be 8 cm^{-1},[62] and the elongated form to be a minimum.

Similarly to the $C_5H_5^{\bullet}$, no warping of the Mexican hat in $C_7H_7^{\bullet}$ is observed, and $^2A_2$ and $^2B_1$ states are isoenergetic, Table 3. E_{JT} obtained by multideterminantal DFT (853.3 cm^{-1}) falls in the range of values previously obtained until now.[19−21]

In all cases, E_{JT} obtained from IDP analysis is in a good agreement with DFT calculations. IDP analysis gives further insight into the vibronic coupling in these JT active molecules. On the potential energy profile it is possible to distinguish two distinct regions (Figures 4a, 5a, 6a). In the first region the energy is changing faster, and depending on the particular molecule, after 25−40% of the path most of the E_{JT} is obtained. An analysis of the multimode JT distortion shows that, regardless of the number of totally symmetric normal modes in LS minimum energy conformation, Table 1, three vibrations are most important for the distortion and for the E_{JT}: C−C stretch, C−C−C bend, and C−C−H bend (Figures 4a, 5a, and 6a, Table 4). A complete analysis of the multimode JT problem at HS point of these molecules is given in the Supporting Information (Tables S1, S2, and S3). The origin of the totally symmetric normal modes in the LS point group, as seen in Table 1, is obtained by correlating them with the normal modes of the parent, non-JT active molecule.[40]

Curiously, the most important JT distortion initially is the hardest of the three modes, the C−C stretch while in the second

Table 5. Results of the DFT Calculations Performed To Analyze the JT Effect in $C_6H_6^{-\,a}$

occupation	state	geometry	energy
$e_{2u}{}^{0.5}e_{2u}{}^{0.5}$	$^2E_{2u}$	D_{6h}	−79.1967
$b_{1u}{}^0a_u{}^1$	^2A_u	D_{6h}	−79.1919
$a_u{}^0b_{1u}{}^1$	$^2B_{1u}$	D_{6h}	−79.1936
$a_u{}^1b_{1u}{}^0$	^2A_u	D_{2h}	−79.2897
$b_{1u}{}^1a_u{}^0$	$^2B_{1u}$	D_{2h}	−79.2847
$a_1{}^1a_1{}^0$	$^2A_1$	C_2	−79.3391
a^1a^0	^2A	D_2	−79.3333
E_{JT}	^2A_u		788.0
E_{JT}	$^2B_{1u}$		735.6
Δ			38.7
R_{JT}	^2A_u		0.19
R_{JT}	$^2B_1$		0.19
$E_{JT/PJT}$	$^2A_1$		1187.3
$E_{JT/PJT}$	^2A		1126.8
Δ			46.8
$R_{JT/PJT}$	$^2A_1$		0.62
$R_{JT/PJT}$	^2A		0.57
$E_{JT}(IDP)$	^2A_u		779.2
$E_{JT}(IDP)$	^2B_u		823.6
$E_{JT/PJT}(IDP)$	^2A_u		1060.5
$E_{JT/PJT}(IDP)$	^2B_u		1009.7

^{a} Energies (LDA) are given in eV; the JT parameters E_{JT} and Δ are given in cm^{-1} and R_{JT} in (amu)$^{1/2}$ Å.

region, where the system relaxes toward the global minimum, softer modes become more important, and the adiabatic potential energy surface is flat. Monitoring changes of all the energy components along the IDP, eqs 8 and 9, gives a whole picture of what happens inside the molecule during the JT distortion. The results are presented in Figure 4c,d for $C_5H_5^{\bullet}$, Figure 5c,d for $C_6H_6^+$, and in Figure 6c,d for $C_7H_7^{\bullet}$. Curves have been displaced vertically to make each energy component zero for the HS configuration, so that the stabilizing and destabilizing interactions along the distortion path can be clearly identified. A similar trend of the changes of energy components is observed for all of the molecules. Two regions are clearly differentiated in the $\Delta T/\Delta V$ profiles. Most of the total energy stabilization is achieved around the HS point when the distortion is driven by the lowering of ΔV and simultaneous increase of ΔT. The initial downward push is clearly due to the Jahn−Teller effect, which is due to the stabilization of the V_{elst}, and the C−C stretch is mainly involved in the distortion. After that the contribution of the C−C stretch drops to the zero. The origin of this distortion is clearly associated to the electron−nuclear interaction, as in Figure 4, and occurs along the C−C stretch, as the active electrons occupy the space between the carbon atoms (see Figure 3). Changes in the V_{XC} energy are an order of magnitude smaller than changes of the V_{elst} and are not important for the qualitative picture. This is in agreement with our experience that the choice of the exchange-correlation functional is not crucial in the DFT studies of the JT effect.[22,31] The kinetic energy apparently favors the HS nuclear configuration. Changes in the T_s are directed with the changes of the T_p, which can be identified as the main opposing contribution to the JT distortion. If we look in more detail into changes of the V_{elst}, it can be seen that the main stabilization comes from the V_{en} which goes quickly down, to adapt to
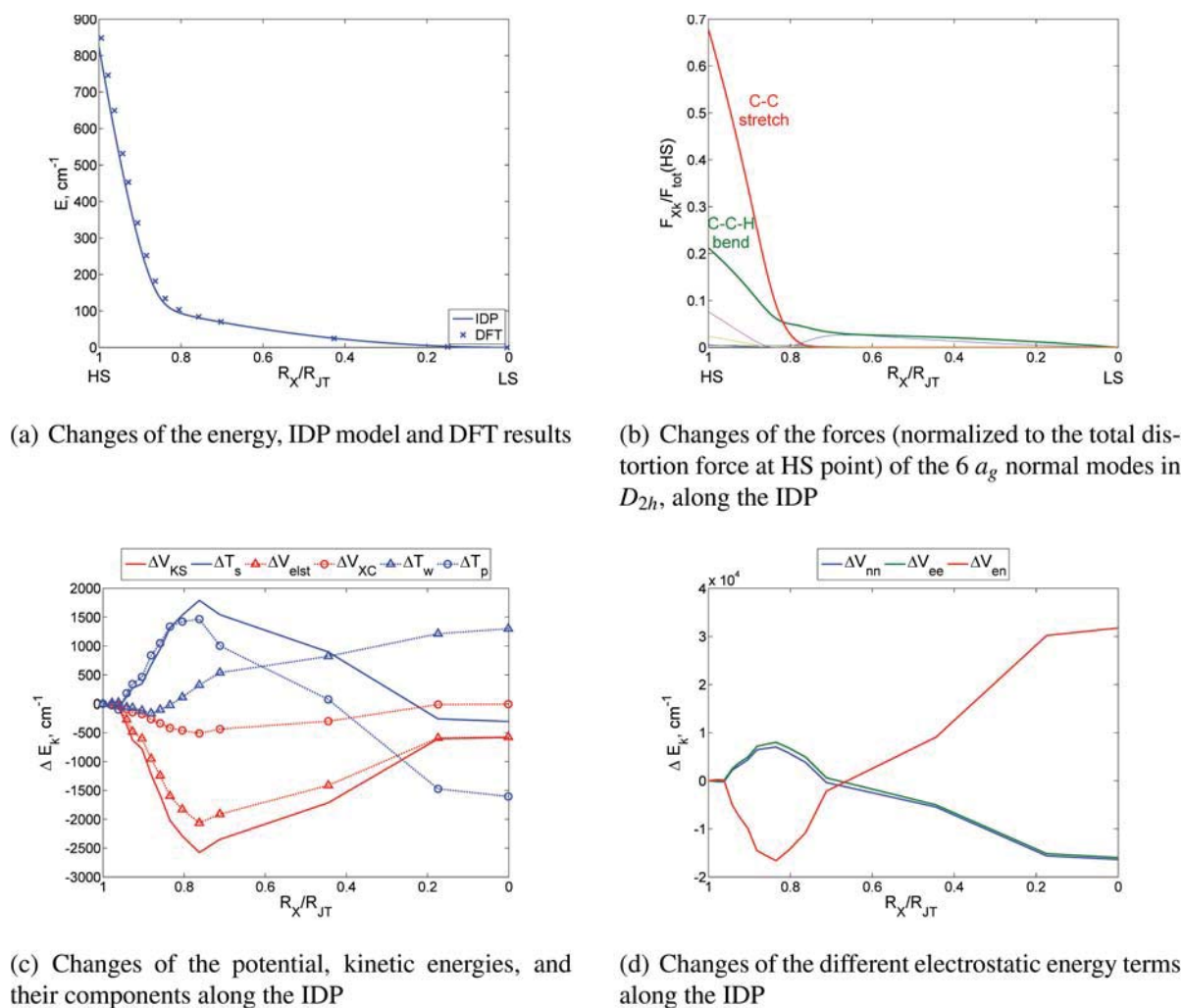
(a) Changes of the energy, IDP model and DFT results

(b) Changes of the forces (normalized to the total distortion force at HS point) of the 6 a_g normal modes in D_{2h}, along the IDP

(c) Changes of the potential, kinetic energies, and their components along the IDP

(d) Changes of the different electrostatic energy terms along the IDP

Figure 7. Intrinsic distortion path and energy component analysis of the JT $D_{6h} \rightarrow D_{2h}$ distortion in $C_6H_6{}^-$.

the nontotally symmetrical electron density, as expected from the theoretical considerations. Two other electrostatic contributions, V_{ee} and V_{nn}, show the opposite tendency, thus giving in total smaller changes in the V_{elst}.

However, after the initial push, the system reaccommodates leading to the strong reduction of the T_p, V_{ee}, and V_{nn}. While T_w almost did not change in the first region, it becomes destabilizing in the second region, and it is changed then parallel to the changes in the V_{elst}. Owing to this behavior of T_w, the total kinetic energy does not contribute globally to stabilize the system. On the other hand the T_p, V_{ee}, and V_{nn} repulsions clearly stabilize the system in the final run. In fact, the energy contribution due to the V_{en} interactions at the end is positive, and the global stabilization seems to come from the electron−electron and nuclear readjustment. Obviously, the correct answer can only be obtained from looking at the whole path and understanding the changes undergone by the forces using the previously explained theory. Thus, while the initial distortion is clearly associated with the usual JT distortions, in the second region softer, bending modes play a more important role, due to the changes of the density caused by the modification of the geometry in the first push. This leads to enhancing the effects of energy components with opposite signs, which are almost canceling each

other, yielding to the very small total energy variation. From the point of view of the JT theory, this also underlines the very important role of the PJT effect, associated to the density changes to obtain the final stabilization energy and barriers in JT systems.

Distortion of Benzene Anion. The benzene molecule, C_6H_6, with the D_{6h} nuclear arrangement has a double-degenerate highest occupied molecular orbital (HOMO), e_{1g}, and a double-degenerate lowest unoccupied molecular orbital (LUMO), e_{2u}. Therefore, $C_6H_6{}^-$ is JT unstable. $C_6H_6{}^-$ has $^2E_{2u}$ ground electronic state in conformation that belongs to the D_{6h} point group. As in the case of $C_6H_6{}^+$, the distortion coordinate is e_{2g} $\left(E_{2u} \times E_{2u} \subset A_{1g} + [A_{2g}] + E_{2g}\right)$, and hence very similar distortion for both cases is expected. DFT results for the anion are presented in Table 5.

After the descent in symmetry to D_{2h}, the electronic state splits into $^2B_{1u}$ and ^2A_u. The latter one is more stable for $\Delta = 38.7$ cm^{-1}, as in Table 5. E_{JT} is bit smaller than in the case of the cation, $E_{JT} = 788$ cm^{-1}. As it can be seen from Table 5, the D_{2h} structure is not the most stable conformation of $C_6H_6{}^-$, and further reduction of symmetry occurs.

Out of six totally symmetric normal modes in the D_{2h} point group, similar to the case of the cation, the influence of the three
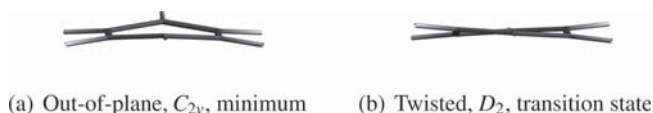
(a) Out-of-plane, C_{2v}, minimum   (b) Twisted, D_2, transition state

Figure 8. Graphical representation of the out-of-plane, C_{2v}, conformation (a) and twisted, D_2, conformation (b) of $C_6H_6^-$.

normal modes is most significant. The IDP method for the JT distortion of $C_6H_6^-$, in Figure 7, reveals the same trend as in the previous cases. The distortion starts with the C—C stretch ($\tilde{\nu}(D_{2h}) = 1496\ cm^{-1}$, 23.27% to the R_{JT}, 69.16% to the E_{JT}), in Figure 7b, and with stabilization of the electron—nuclear attraction Figure 7d. After 20% of the path, most of the energy stabilization is achieved, as in Figure 7a. In the second region there is a strong reduction of the electron—electron, nuclear—nuclear, and Pauli kinetic energy. The difference to the case of cation is that the C—C—C bending is not as important ($\tilde{\nu}(D_{2h}) = 604\ cm^{-1}$, 9.58% to the R_{JT}, 5.21% to the E_{JT}), and C—C—H bending is dominating in this region ($\tilde{\nu}(D_{2h}) = 1093\ cm^{-1}$, 64.63% to the R_{JT}, 22.21% to the E_{JT}), as in Figure 7d. A detailed analysis of the multimode JT effect at the HS point is given in Table S4 in the Supporting Information.

DFT calculations show even further differences between the electronic structure of the benzene cation and anion. In the case of anion, LUMO, both in the D_{6h} and in D_{2h} configurations, is σ^* (a_{1g}) MO and not π^* as it could be expected from the electronic structure of the neutral benzene. Thus, the first excited state of anion is $^2A_{1g}$ which is estimated to lie only around 0.1 eV above the ground $^2E_{2u}$ state in a D_{6h} configuration and 0.7 eV above the ground states in D_{2h} configurations. Due to the PJT coupling of the ground, π^* electronic state with the excited σ^* state, DFT frequency calculations reveal one imaginary e_{2u} frequency in D_{6h}, one a_u imaginary frequency in ^2A_u D_{2h} structure, and two imaginary frequencies in ^2B_u, one b_{1u} and one b_{1g} (pseudo-rotation around the JT cusp). Following the imaginary frequencies, the true stationary points on the adiabatic potential energy surface were obtained. The out-of-plane C_{2v} conformation, in Figure 8a, is the global minimum, which lies around 400 cm^{-1} below the planar D_{2h} structures. The out-of-plane conformation is more stable than the twisted D_2 conformation, in Figure 8b, for 47 cm^{-1}. This situation is similar to the case of $C_6F_6^-$.[63] The relation between the structures of D_{2h}, C_{2v}, and D_2 symmetry on the adiabatic potential energy surface is schematically shown in Figure 9. Twisted D_2 and planar $D_{2h}(^2A_u)$ conformations are saddle points on the adiabatic potential energy surface. $D_{2h}(^2B_{1u})$ planar conformation is second-order saddle point on the adiabatic potential energy surface, which is indicated with dashed arrows in Figure 9. Both C_{2v} and D_2 point groups are subgroups of D_{2h} and D_{6h} point groups, and the puckering and twisting of $C_6H_6^-$ are consequence of the combined JT and PJT effects.

To analyze the combined JT and PJT distortion of $C_6H_6^-$, $D_{6h} \rightarrow C_{2v}$ distortion, it is necessary to consider nine totally symmetric normal modes in C_{2v} minimum energy conformation. They correlate to the four e_{2g}, two a_{1g}, two b_{2u}, and one e_{2u} vibration in D_{6h}. Even though this distortion is more complicated than previously discussed cases, E_{JT} obtained from the IDP analysis, 1060 cm^{-1}, is still in rather good agreement with the value of 1187 cm^{-1} from multideterminantal DFT calculations. Two distinct regions on the adiabatic potential energy surface could be distinguished, in Figure 10a. Very early along the IDP, c. a. after 5% of the path, a strong stabilization of around 500 cm^{-1} is achieved. In this region C—C stretch ($\tilde{\nu}(C_{2v}) = 1531\ cm^{-1}$,
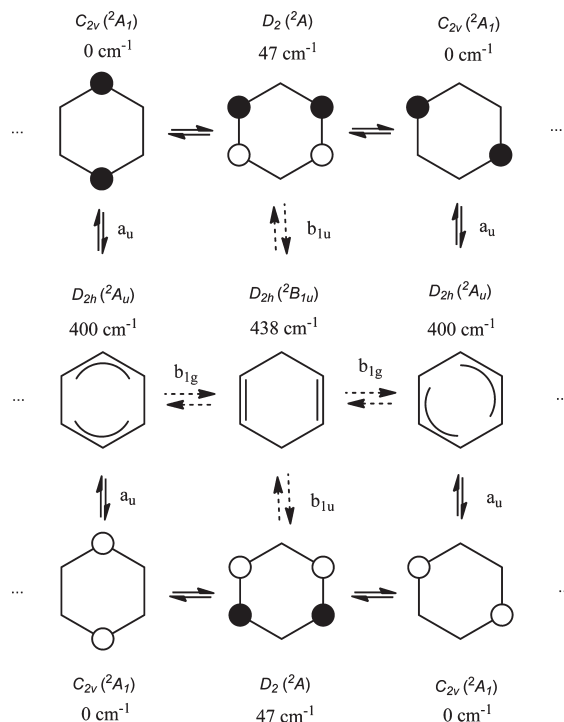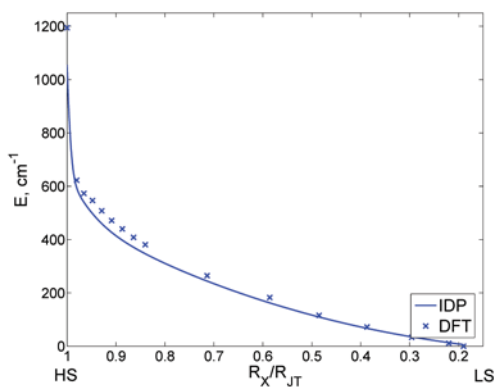

Figure 9. Relation between various structures of $C_6H_6^-$; open (white) and closed (black) circles represent carbon atoms lying below and above the mean plane of the $C_6H_6^-$; energies are given relative to the global minimum, C_{2v} structure, in cm^{-1}; D_{6h} structure lies 1190 cm^{-1} above the global minimum; the symmetry of the vibrations with negative force constants in D_{2h} structures and their direction is indicated.
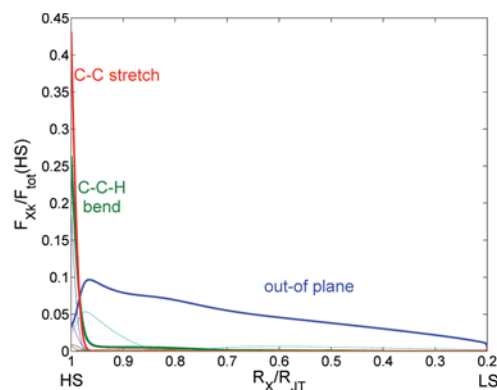
1.3% to the R_{JT}, 25.9% to the E_{JT+PJT}) and C—C—H bending ($\tilde{\nu}(C_{2v}) = 1112\ cm^{-1}$, 3.9% to the R_{JT}, 10.4% to the E_{JT+PJT}) are dominating, in Figure 10b. So, in this region, there is a proper JT distortion, similar to the previously described cases. In the second region the adiabatic energy surface is not flat, and energy gradually decreases for additional 500 cm^{-1}. In this region distortion is almost completely described with the out-of-plane normal mode ($\tilde{\nu}(C_{2v}) = 320\ cm^{-1}$, 90.9% to the R_{JT}, 51.2% to the E_{JT+PJT}). This out-of-plane vibration correlates to the modes with imaginary frequencies in D_{6h} or D_{2h} structures. All of the other vibrations have negligible influence on the both the distortion and the stabilization, as in Table S5 in the Supporting Information. The total stabilization energy is due to the stabilization of the electron—nuclear attraction along the path. This is because PJT $\pi^* - \sigma^*$ mixing introduces additional bonding within a molecule. T_w and V_{XC} are also getting stabilized, while other energy components are opposing to the distortion, as in Figure 10c,d.
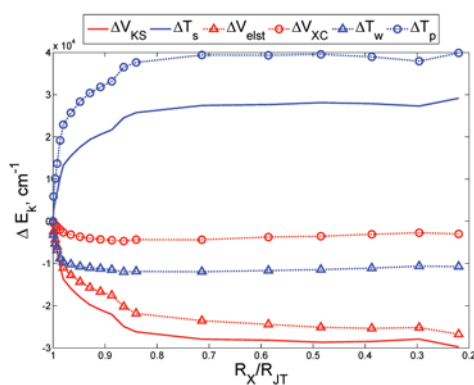
■ CONCLUSIONS

In this paper, a general approach to analyze the multimode JT problem is presented and applied using the multideterminantal DFT method to study the adiabatic potential energy surface of the family of JT active hydrocarbon rings, C_nH_n ($n = 5-7$). The essence of the model is to express the distortion along the steepest descent path as a linear combination of all totally symmetric normal modes in LS minimum energy conformation and then perform an analysis of the contributions to the energy. The IDP analysis answers the questions of which are the
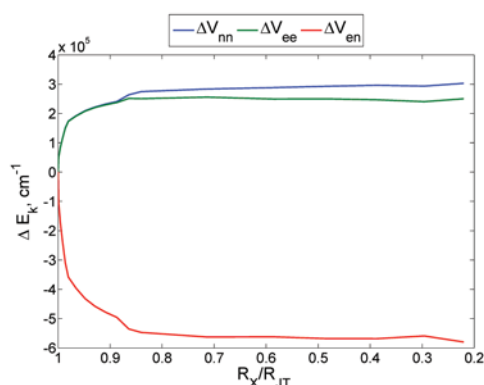
(a) Changes of the energy, IDP model and DFT results

(b) Changes of the forces (normalized to the total distortion force at HS point) of the 9 a_1 normal modes in C_{2v}, along the IDP

(c) Changes of the potential and kinetic energies along the IDP

(d) Changes of the different potential energy terms along the IDP

Figure 10. Intrinsic distortion path and energy component analysis of the combined JT/PJT $D_{6h} \rightarrow C_{2v}$ distortion in $C_6H_6^{-}$.

totally symmetric normal modes of the LS structure that contribute to the JT distortion at the HS point, how they contribute to the E_{JT}, and how their contributions change along the IDP. Additionally the examination of the systematic effects in the shape of the potential energy surfaces in these aromatic rings was elucidated.

All considered molecules have a doubly degenerate electronic ground state which is coupled with vibrations of doubly degenerate irreps in the HS point group. Although the nature of chemical bonding is the same in all systems, they differ in the symmetry of the distortion, range of E_{JT}, the number of atoms, and hence the number of different normal modes that need to be considered in the IDP analysis. The results obtained by multi-determinantal DFT and IDP methods are in a good agreement with the theoretical and experimentally estimated values reported in the literature so far. These results demonstrate the utility of this methodology, not only for the analysis of the proper JT effect, but also when PJT coupling is present. However, IDP method has not yet been explored in the cases where PJT or hidden JT effect[64] determine a structure. The combination of the alternative methods for the analysis of the multimode problem, one starting from the HS nuclear configuration and reduction of the multimode problem to a single interaction mode[2,26] and IDP method starting from the LS nuclear configuration may be a possible general solution of the multimode problem and can be considered to become reliable tools for a better understanding of the JT phenomena.

The inspection of the IDP indicates that linearly JT active vibrations dominate along the path; harder ones are most important in the beginning, while softer ones take over along the path. Totally symmetric type vibrations appear not to be important. The contribution to the E_{JT} mainly originates from C−C stretch normal modes in C_nH_n molecules. The energy component analysis revealed that, while the electron−nuclear interactions are very important in the stabilization of the system around the high-symmetry point, other forces due to the electron−electron, nuclear−nuclear, and kinetic interactions are dominant in later stages of the distortion, although contributing very little to the total stabilization of the molecule through bending deformations. It can be concluded that, looking only at the values of individual energy components at HS and LS structures, without analyzing the details of their changes along the distortion path, chemically important features could be lost, and even wrong conclusions could be drawn. The correct answer can be obtained by inspection of the IDP, monitoring the changes of the contributions of the most important normal modes, in conjunction with energy component analysis. The subtle changes of the energy components are emerging as the outcome of the

multimode JT effect in combination with changes in the electron density through the PJT effect.

The assessment of the changes of individual energy components, in the combination with the IDP analysis of the multimode JT problem, gives an information about the main driving force for the distortion. This helps to rationalize the influence of different movements of nuclei on the electron density in a molecule.

■ ASSOCIATED CONTENT

Ⓢ Supporting Information. Complete analysis of the multimode JT effect in the HS points on the adiabatic potential energy surfaces of $C_5H_5^\bullet$, $C_6H_6^+$, $C_7H_7^\bullet$, and $C_6H_6^-$ by the LS totally symmetric normal modes in a harmonic approximation—IDP analysis at the HS points.

■ AUTHOR INFORMATION

Corresponding Author
*E-mail: matijaz@chem.bg.ac.rs.

■ ACKNOWLEDGMENT

■ REFERENCES

(1) Jahn, H. A.; Teller, E. *Proc. R. Soc. London, Ser. A* **1937**, *161*, 220–235.

(2) Bersuker, I. B. *The Jahn-Teller Effect*; Cambridge University Press: New York, 2006.

(3) Renner, R. *Z. Phys. A* **1934**, *92*, 172–193.

(4) (a) Bersuker, I. B. *Electronic Structure and Properties of Transition Metal Compounds*; J. Wiley and Sons: New York, 2010. (b) Köppel, H.; Yarkony, D. R.; Barentzen, H., Eds. *The Jahn-Teller Effect, Fundamentals and Implications for Physics and Chemistry*; Springer Series in Chemical Physics, Vol. 97; Springer: New York, 2009. (c) O'Brien, M. C. M.; Chancey, C. C. *Am. J. Phys.* **1993**, *61*, 688–697. (d) Bersuker, I. B.; Polinger, V. Z. *Vibronic Interactions in Molecules and Crystals*; Springer-Verlag: Berlin, 1989. (e) Pearson, R. G. *Symmetry Rules for Chemical Reactions*; Wiley-Interscience Publications: New York, 1976.

(5) (a) Bednorz, J. G.; Müler, K. A. *Z. Phys. B: Condens. Matter* **1986**, *64*, 189–193. (b) Bednorz, J. G.; Müler, K. A. In *Nobel Lectures: Physics 1981−1990*; Ekspang, G., Ed.; World Scientific Publishing Co.: Singapore, 1993; pp 424−457.

(6) Millis, A. J. *Nature* **1998**, *392*, 147–150.

(7) (a) Applegate, B. E.; Miller, T. A. *J. Chem. Phys.* **2001**, *114*, 4855–4869. (b) Applegate, B. E.; Bezant, J.; Miller, T. A. *J. Chem. Phys.* **2001**, *114*, 4869–4882.

(8) Zilberg, S.; Haas, Y. *J. Am. Chem. Soc.* **2002**, *124*, 10683–10691.

(9) Sato, T.; Tanaka, K.; Tokunaga, K. *J. Chem. Phys.* **2006**, *124*, 024314.

(10) Ichino, T.; Wren, S. W.; Vogelhuber, K. M.; Gianola, A. J.; Lineberger, W. C.; Stanton, J. F. *J. Chem. Phys.* **2008**, *129*, 084310–084319.

(11) Zlatar, M.; Schläpfer, C.-W.; Daul, C. In *The Jahn-Teller-Effect Fundamentals and Implications for Physics and Chemistry*; Koeppel, H., Yarkoni, D. R., Barentzen, H., Eds.; Springer Series in Chemical Physics, Vol. 97; Springer: New York, 2009; pp 131−165.

(12) Muller-Dethlefs, K.; Peel, J. B. *J. Chem. Phys.* **1999**, *111*, 10550–10554.

(13) Applegate, B. E.; Miller, T. A. *J. Chem. Phys.* **2002**, *117*, 10654–10674.

(14) Perebeinos, V.; Allen, P. B.; Pederson, M. *Phys. Rev. A* **2005**, *72*, 012501.

(15) Tokunaga, K.; Sato, T.; Tanaka, K. *J. Chem. Phys.* **2006**, *124*, 154303.

(16) (a) Köppel, H.; Cederbaum, L. S.; Domcke, W. *J. Chem. Phys.* **1988**, *89*, 2023–2040. (b) Döscher, M.; Köppel, H.; Szalay, P. G. *J. Chem. Phys.* **2002**, *117*, 2645–2656. (c) Döscher, M.; Köppel, H.; Baldea, I.; Meyer, H.-D.; Szalay, P. G. *J. Chem. Phys.* **2002**, *117*, 2657–2671. (d) Baldea, I.; Köppel, H. *J. Chem. Phys.* **2006**, *124*, 064101.

(17) Sardar, S.; Paul, A. K.; Sharma, R.; Adhikari, S. *J. Chem. Phys.* **2009**, *130*, 144302.

(18) Gunion, R. F.; Karney, W.; Wenthold, P. G.; Borden, W. T.; Lineberger, W. C. *J. Am. Chem. Soc.* **1996**, *118*, 5074–5082.

(19) (a) Stakhursky, V. L.; Sioutis, I.; Tarczay, G.; Miller, T. A. *J. Chem. Phys.* **2008**, *128*, 084310. (b) Sioutis, I.; Stakhursky, V. L.; Tarczay, G.; Miller, T. A. *J. Chem. Phys.* **2008**, *128*, 084311.

(20) Yi, H.; Lee, H.; Suh, S. B. *J. Chem. Phys.* **2006**, *125*, 164332.

(21) Pino, T.; Güthe, F.; Ding, H.; Maier, J. P. *J. Phys. Chem. A* **2002**, *106*, 10022–10026.

(22) (a) Bruyndonckx, R.; Daul, C.; Manoharan, P. T.; Deiss, E. *Inorg. Chem.* **1997**, *36*, 4251–4256. (b) Kundu, T. K.; Bruyndonckx, R.; Daul, C.; Manoharan, P. T. *Inorg. Chem.* **1999**, *38*, 3931–3934.

(23) (a) Zlatar, M.; Schläpfer, C.-W.; Fowe, E. P.; Daul, C. *Pure Appl. Chem.* **2009**, *81*, 1397–1411. (b) Zlatar, M.; Gruden-Pavlović, M.; Schläpfer, C.-W.; Daul, C. *J. Mol. Struct.: THEOCHEM* **2010**, *954*, 86–93. (c) Gruden-Pavlović, M.; Zlatar, M.; Schläpfer, C.-W.; Daul, C. *J. Mol. Struct.: THEOCHEM* **2010**, *954*, 80–85. (d) Zlatar, M.; Gruden-Pavlović, M.; Schläpfer, C.-W.; Daul, C. *Chimia* **2010**, *64*, 161–164.

(24) (a) Ceulemans, A; Vanquickenborne, L. G. *Struct. Bonding (Berlin)* **1989**, *71*, 125–159. (b) Ceulemans, A; Beyens, D.; Vanquickenborne, L. G. *J. Am. Chem. Soc.* **1984**, *106*, 5824–5837.

(25) García-Fernández, P.; Bersuker, I. B.; Aramburu, J. A.; Barriuso, M. T.; Moreno, M. *Phys. Rev. B* **2005**, *71*, 184117–1−10.

(26) Liu, Y.; Bersuker, I. B.; Zou, W.; Boggs, J. E. *J. Chem. Theory Comput.* **2009**, *5*, 2679–2686.

(27) Liu, S. *J. Chem. Phys.* **2007**, *126*, 244103.

(28) Clinton, W. L.; Rice, B. *J. Chem. Phys.* **1959**, *30*, 542–546.

(29) García-Lastra, J. M.; Barriuso, M. T.; Aramburu, J. A.; Moreno, M. *Chem. Phys.* **2005**, *317*, 103–110.

(30) Reinen, D.; Atanasov, M.; Massa, W. *Z. Anorg. Allg. Chem.* **2006**, *632*, 1375–1398.

(31) (a) Atanasov, M.; Comba, P. *J. Mol. Struct.* **2007**, *38*, 157–163. (b) Atanasov, M.; Comba, P.; Daul, C. A.; Hauser, A. *J. Phys. Chem. A* **2007**, *38*, 9145–9163. (c) Barriuso, M. T.; García-Fernández, P.; Aramburu, J. A.; Moreno, M. *Int. J. Quantum Chem.* **2003**, *91*, 202–207.

(32) Aramburu, J.; Barriuso, M.; Garcia-Fernandez, P.; Moreno, M. *Adv. Quantum Chem.* **2004**, *44*, 445–459.

(33) Reinen, D.; Atanasov, M.; Köhler, P.; Babel, D. *Coord. Chem. Rev.* **2010**, *254*, 2703–2754.

(34) (a) Bersuker, I. B. *J. Comput. Chem.* **1997**, *18*, 260–267. (b) Kaplan, I. G. *J. Mol. Struct.* **2007**, *838*, 39–43.

(35) Atanasov, M.; Daul, C. *Chimia* **2005**, *59*, 504–510.

(36) (a) Baerends, E. J. et al. *ADF2009.01*. http://www.scm.com, 2009. (b) Guerra, C. F.; Snijders, J. G.; te Velde, G.; Baerends, E. J. *Theor. Chem. Acc.* **1998**, *99*, 391–403. (c) te Velde, G.; Bickelhaupt, F. M.; van Gisbergen, S. J. A.; Guerra, C. F.; Baerends, E. J.; Snijders, J. G.; Ziegler, T. *J. Comput. Chem.* **2001**, *22*, 931–967.

(37) Vosko, S.; Wilk, L.; Nusair, M. *Can. J. Phys.* **1980**, *58*, 1200–1211.

(38) Swart, M.; Bickelhaupt, F. M. *J. Comput. Chem.* **2007**, *29*, 724–734.

(39) (a) Bérces, A.; Dickson, R. M.; Fan, L.; Jacobsen, H.; Swerhone, D.; Ziegler, T. *Comput. Phys. Commun.* **1997**, *100*, 247–262. (b) Jacobsen, H.; Bérces, A.; Swerhone, D.; Ziegler, T. *Comput. Phys. Commun.* **1997**, *100*, 263–276.

(40) (a) Hug, W.; Fedorovsky, M. *Theor. Chem. Acc.* **2008**, *119*, 113–131. (b) Fedorovsky, M. PyVib2, a program for analyzing vibrational motion and vibrational spectra. http://pyvib2.sourceforge.net, 2007.

(41) (a) Ruedenberg, K. *Rev. Mod. Phys.* **1962**, *34*, 326–376. (b) Feinberg, M. J.; Ruedenberg, K. *J. Chem. Phys.* **1971**, *54*, 1495–1511.

(c) Bitter, T.; Ruedenberg, K.; Schwarz, W. H. E. *J. Comput. Chem.* **2007**, *28*, 411–422.

(42) (a) Boyd, R. J. *Nature* **1984**, *310*, 480–481. (b) Zhong, A.; Liu, S. *J. Theor. Comput. Chem.* **2005**, *4*, 833–847. (c) Oyamada, T.; Hongo, K.; Kawazoe, Y.; Yasuhara, H. *J. Chem. Phys.* **2010**, *133*, 164113.

(43) (a) Ichikawa, H.; Ebisawa, Y. *J. Am. Chem. Soc.* **1985**, *107*, 1161–1165. (b) Ichikawa, H.; Kagawa, H. *J. Phys. Chem.* **1995**, *99*, 2307–2311.

(44) Rong, C.; Lian, S.; Yin, D.; Shen, B.; Zhong, A.; Bartolotti, L.; Liu, S. *J. Chem. Phys.* **2006**, *125*, 174102.

(45) (a) Toyota, A.; Koseki, S. *J. Phys. Chem.* **1996**, *100*, 2100–2106. (b) Koseki, S.; Toyota, A. *J. Phys. Chem. A* **1997**, *101*, 5712–5718. (c) Toyota, A.; Koseki, S. *J. Phys. Chem. A* **1998**, *102*, 490–495. (d) Toyota, A.; Koseki, S. *J. Phys. Chem. A* **1998**, *102*, 6668–6675. (e) Toyota, A.; Koseki, S.; Shiota, M. *J. Phys. Chem. A* **2000**, *104*, 5343–5350. (f) Toyota, A.; Shiota, M.; Nagae, Y.; Koseki, S. *J. Phys. Chem. A* **2001**, *105*, 1334–1342. (g) Toyota, A.; Koseki, S.; Umeda, H.; Suzuki, M.; Fujimoto, K. *J. Phys. Chem. A* **2003**, *107*, 2749–2756.

(46) Garcia-Fernandez, P.; Aramburu, J.; Barriuso, M.; Moreno, M. *J. Phys. Chem. Lett.* **2010**, *1*, 647–651.

(47) (a) Liu, S.; Govind, N.; Pedersen, L. G. *J. Chem. Phys.* **2008**, *129*, 094104. (b) Liu, S.; Govind, N. *J. Phys. Chem. A* **2008**, *112*, 6690–6699. (c) Ugur, I.; De Vleeschouwer, F.; Tüzün, N.; Aviyente, V.; Geerlings, P.; Liu, S.; Ayers, P. W.; De Proft, F. *J. Phys. Chem. A* **2009**, *113*, 8704–8711. (d) Liu, S.; Hu, H.; Pedersen, L. G. *J. Phys. Chem. A* **2010**, *114*, 5913–5918. (e) Ess, D. H.; Liu, S.; De Proft, F. *J. Phys. Chem. A* **2010**, *114*, 12952–12957. (f) Huang, Y.; Zhong, A.-G.; Yang, Q.; Liu, S. *J. Chem. Phys.* **2011**, *134*, 084103.

(48) (a) Boyd, R. J.; Darvesh, K. V.; Fricker, P. D. *J. Chem. Phys.* **1991**, *94*, 8083–8088. (b) Wang, J.; Boyd, R. J. *J. Chem. Phys.* **1992**, *96*, 1232–1239. (c) Proft, F. D.; Geerlings, P. *Chem. Phys. Lett.* **1996**, *262*, 782–788.

(49) Kohn, W.; Sham, L. J. *Phys. Rev.* **1965**, *140*, A1133–A1138.

(50) Parr, R. G.; Yang, W. *Density-Functional Theory of Atoms and Molecules*; Oxford University Press: New York, 1989.

(51) (a) Liu, S.; Parr, R. G. *Phys. Rev. A* **1996**, *53*, 2211–2219. (b) Rodríguez, J. I.; Ayers, P. W.; Götz, A. W.; Castillo-Alvarado, F. L. *J. Chem. Phys.* **2009**, *131*, 021101.

(52) Weizsäcker, C. F. v. *Z. Phys. A: Hadrons Nuclei* **1935**, *96*, 431–458.

(53) (a) March, N. H. *Phys. Lett. A* **1986**, *113*, 476–478. (b) Levy, M.; Ou-Yang, H. *Phys. Rev. A* **1988**, *38*, 625–629. (c) Herring, C. *Phys. Rev. A* **1986**, *34*, 2614–2631. (d) Herring, C.; Chopra, M. *Phys. Rev. A* **1988**, *37*, 31–42. (e) Holas, A.; March, N. H. *Phys. Rev. A* **1991**, *44*, 5521–5536. (f) Nagy, A. *Int. J. Quantum Chem.* **2010**, *110*, 2117–2120.

(54) Zhao, Q.; Parr, R. G. *Phys. Rev. A* **1992**, *46*, 2337–2343.

(55) Weisskopf, V. F. *Science* **1975**, *187*, 605–612.

(56) Bader, R. *Atoms in Molecules: A Quantum Theory*; Clarendon Press: Oxford, U.K., 1994.

(57) (a) Liu, S. *J. Chem. Phys.* **2007**, *126*, 191107. (b) Esquivel, R. O.; Liu, S.; Angulo, J. C.; Dehesa, J. S.; Antolin, J.; Molina-Espiritu, M. *J. Phys. Chem. A* **2011**, *115*, 4406–4415.

(58) (a) Becke, A. D.; Edgecombe, K. E. *J. Chem. Phys.* **1990**, *92*, 5397–5403. (b) Savin, A.; Jepsen, O.; Flad, J.; Andersen, O. K.; Preuss, H.; von Schnering, H. G. *Angew. Chem. Int. Ed. Engl.* **1992**, *31*, 187–188.

(59) Valiev, M.; Bylaska, E.; Govind, N.; Kowalski, K.; Straatsma, T.; Dam, H. V.; Wang, D.; Nieplocha, J.; Apra, E.; Windus, T.; de Jong, W. *Comput. Phys. Commun.* **2010**, *181*, 1477–1489.

(60) (a) Hellmann, H. *Einführung in die Quantenchemie*; Leipzig: Franz Deuticke, 1937. (b) Feynman, R. P. *Phys. Rev.* **1939**, *56*, 340–343.

(61) Coulson, C. A.; Bell, R. P. *Trans. Faraday Soc.* **1945**, *41*, 141–149.

(62) Lindner, R.; Müller-Dethlefs, K.; Wedum, E.; Haber, K.; Grant, E. R. *Science* **1996**, *271*, 1698–1702.

(63) Shchegoleva, L. N.; Beregovaya, I. V.; Schastnev, P. V. *Chem. Phys. Lett.* **1999**, *312*, 325–332.

(64) (a) Garcia-Fernandez, P.; Bersuker, I. B.; Boggs, J. E. *Phys. Rev. Lett.* **2006**, *96*, 163005. (b) Bersuker, I. B. In *The Jahn-Teller-Effect Fundamentals and Implications for Physics and Chemistry*; Koeppel, H., Yarkoni, D. R., Barentzen, H., Eds.; Springer Series in Chemical Physics, Vol. 97; Springer: New York, 2009; pp 3–23; (c) Garcia-Fernandez, P.; Bersuker, I. B. *Phys. Rev. Lett.* **2011**, *106*, 246406.